

# Inorganic electrochromic metasurface in the visible

*Yohan Lee<sup>1\*</sup>, Jonas Herbig<sup>1</sup>, Serkan Arslan<sup>1</sup>, Dominik Ludescher<sup>1</sup>, Monika Ubl<sup>1</sup>, Andreas Georg<sup>2</sup>, Mario Hentschel<sup>1</sup>, and Harald Giessen<sup>1\*</sup>*

<sup>1</sup> 4th Physics Institute and Research Center SCoPE, University of Stuttgart, Pfaffenwaldring 57, 70569 Stuttgart, Germany

<sup>2</sup> Fraunhofer Institute for Solar Energy Systems, Heidenhofstraße 2, 79110 Freiburg, Germany

\*Corresponding author, e-mail: [y.lee@pi4.uni-stuttgart.de](mailto:y.lee@pi4.uni-stuttgart.de), [giessen@pi4.uni-stuttgart.de](mailto:giessen@pi4.uni-stuttgart.de)

## **Keywords:**

Inorganic, Electrochromic, Metasurfaces, Electrically Switchable, Full colour switching

## **Abstract:**

Colour printing based on metallic or dielectric nanostructures has revolutionized colour science due to its unprecedented subwavelength resolution. Evidently, the evolution towards the active control of such structural colours with smart materials is in progress for real applications. Here we experimentally demonstrate a large colour gamut with high intensity and purity, as well as its switching on and off based solely on tungsten trioxide (WO<sub>3</sub>) cylindrical resonators. The strong resonances in the visible spectral range in these WO<sub>3</sub> metasurfaces can be reversibly switched on and off due to its electrochromism by applying alternating voltages of +2.0 V and -0.3 V. Our approach opens up possibilities for the functional diversification of commercial smart windows, as well as the development of new display technologies in the future.

## Main manuscript

Colour generation with nanostructures [1,2], has been explored since ancient times in human history, as seen in the well-known Lycurgus Cup, stained glasses, and potteries [3]. Different from applying dyes or pigments as traditional techniques to generate colours, a structural colouration can offer promising opportunities such as vivid and vibrant colours, high durability, precise colour tuning capabilities, and environmental friendliness. Consequently, in the recent decade, there have been extensive efforts employing plasmonic nanostructures towards expanding the colour space and achieving high resolution and saturation, because the resonance can be easily tuned by the structural information including the size, shape, and arrangement of the nanoscatterers with recent advancement in nanofabrication and optical characterization techniques [1]. However, due to the inherent loss of metals in the visible range, the resonance peaks from plasmonic nanostructures are typically broad and less intense, preventing them from truly competing with the colour space of traditional pigments [4-9]. In this context, high-index dielectric nanostructures such as silicon (Si) or titanium dioxide (TiO<sub>2</sub>) have garnered significant attention for nanoscale colour printing, because they can support optical resonances in the visible spectrum through Mie resonances [10-15]. Such materials possess enhanced resonance quality factors related to the saturation of colours due to the absorption losses.

The notable advantage achievable only through structural colour reproduction is the ability to actively control the colour via external stimuli, which is not possible with traditional methods. The realization of such dynamic structural colour is crucial for extending functionality beyond merely static images to include animations. Commonly reported approaches involve employing active materials that respond to physical or chemical principles to alter the refractive index or size of nanoresonators [16-24], or to change the refractive index of the background of nanostructures [25-32]. Previous studies on dynamic structural colours have two main limitations: (1) Most studies have focused on transitions to different colours rather than ON/OFF colour switching [19-27, 30, 31]. For real applications, it is essential to have several basic colours (such as red, green, and blue) that can be turned on and off, along with their combinations, similar to the principle of commercialized displays. (2) The materials used for colour reproduction and the active materials used for colour control are different [28, 29, 32]. Adding other types of materials for active control could introduce compatibility issues or compromise the desired optical properties, potentially reducing the overall efficiency or reliability of the color-changing process.

Here, we introduce an electrically switchable full-colour palette, made from tungsten trioxide (WO<sub>3</sub>) nanostructures based on an electrochemically-driven tuning of its refractive index. The proposed platform consisting of solely one material is able to express a wide colour gamut, as well as to dynamically switch it on and off via an applied voltage.

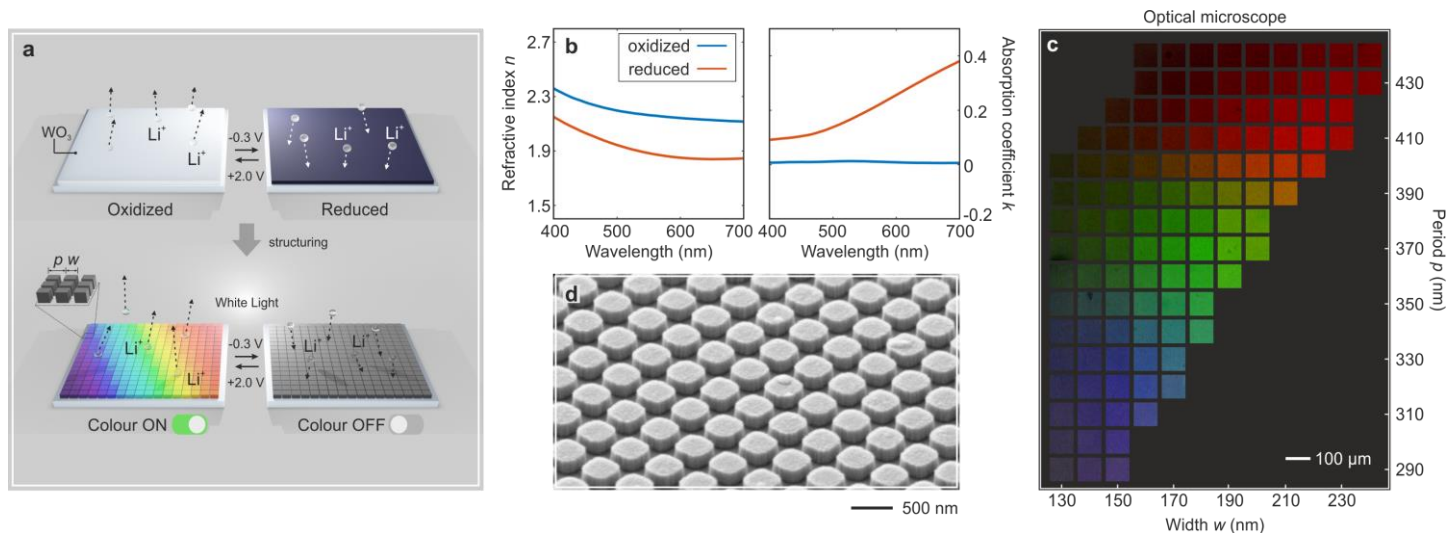
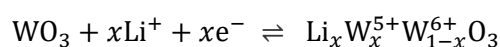


**Figure 1. Concept of full-colour-switchable metasurfaces made from tungsten trioxide (WO<sub>3</sub>).** (a) Schematic of the working principle of the inorganic electrochromic metasurfaces. WO<sub>3</sub> as a thin film shows simple electrochromic property from transparent to deep blue with electrochemically redox reaction (Top). Nanopatterned WO<sub>3</sub> not only allows for the generation of a wide colour gamut depending on the period ( $p$ ) and width ( $w$ ) of nanoresonators, but also allows the colours to be switched on and off at a faster rate (Bottom). (b) Refractive index (Left) and absorption coefficient (Right) of WO<sub>3</sub> at oxidized and reduced states. WO<sub>3</sub> has relatively high refractive index ( $n \approx 2.2$ ) in the visible. Evidently, nearly no absorption is observed at oxidized state in the visible, while electrochemically reduced WO<sub>3</sub> shows dispersive absorption. (c) Optical microscope image with 5x objective of the colour palette made from WO<sub>3</sub> metasurfaces with the combinations of different  $p$  and  $w$ . (d) Scanning electron microscopy (SEM) image shows the WO<sub>3</sub> metasurface with one specific condition of  $p$  and  $w$ .

The concept of our inorganic metasurfaces is illustrated in Figure 1. Pristine WO<sub>3</sub>, utilized in current smart windows, is transparent in its as-deposited film state (Top of Figure 1a). The dynamic behavior of WO<sub>3</sub> is enabled by the unique phenomenon of the material changing colour in response to an electric stimulus, known as electrochromism. Depending on the electrochemical reactions induced by the intercalation or de-intercalation of lithium ions dissolved in an electrolyte, it can exhibit a switch from transparency to a deep blue colour (see Figure S1 in the Supporting Information). This switching mechanism takes place by the following reaction [33].



In this work, we find that nanopatterned WO<sub>3</sub> can express a wide range of colour space with high purity by tailoring the geometric conditions of the patterns, such as period  $p$  and width  $w$  (Bottom of Figure 1a). Furthermore, leveraging the electrochromic phenomenon of the material itself, the brilliant

colours can be switched off and on again by applying voltages of -0.3 V and +2.0 V (versus a reference electrode). The proposed concept shows the novelty that colour generation and switching are simultaneously achieved solely with monolithic WO<sub>3</sub>.

The mechanism of our active metasurfaces relies on the variation of refractive index of WO<sub>3</sub> by applied voltages. Figure 1b depicts the real and imaginary parts of the refractive indices of WO<sub>3</sub> in its oxidized (or pristine) and reduced states (see Table S1 in the supporting Information for detailed values). We notice that in the visible, WO<sub>3</sub> has a sufficiently high refractive index (around 2.2) and nearly no intrinsic losses when it is oxidized, which makes it possible to support highly localized resonance in material. Notably, as WO<sub>3</sub> gets electrochemically reduced by an external voltage, the absorption coefficient of WO<sub>3</sub> (the imaginary part of the refractive index) increases, thereby enabling the suppression of such a resonance.

In Figure 1c, we display the colour palette generated by our WO<sub>3</sub> metasurfaces. Optical images of the colours are taken with a 5x NA 0.15 objective at a fully closed aperture stop, in order to filter out the normal component. (Angle dependency of the metasurfaces is presented in Figure S2 in the Supporting Information.) It is clear that the colours and their intensities are determined by period  $p$  and width  $w$  of the WO<sub>3</sub> nanoresonators. Figure 1d depicts a scanning electron microscope (SEM) image of our WO<sub>3</sub> metasurface taken for one of the structures that have different  $p$  and  $w$ . The nanopattern is a cuboid shape as designed, which shows excellent quality of nanofabrication. Additional SEM images of the structures with various conditions can be found in Figure S3 in the Supporting Information. The detail of nanofabrication is provided in Methods and Figure S4 in the Supporting Information.

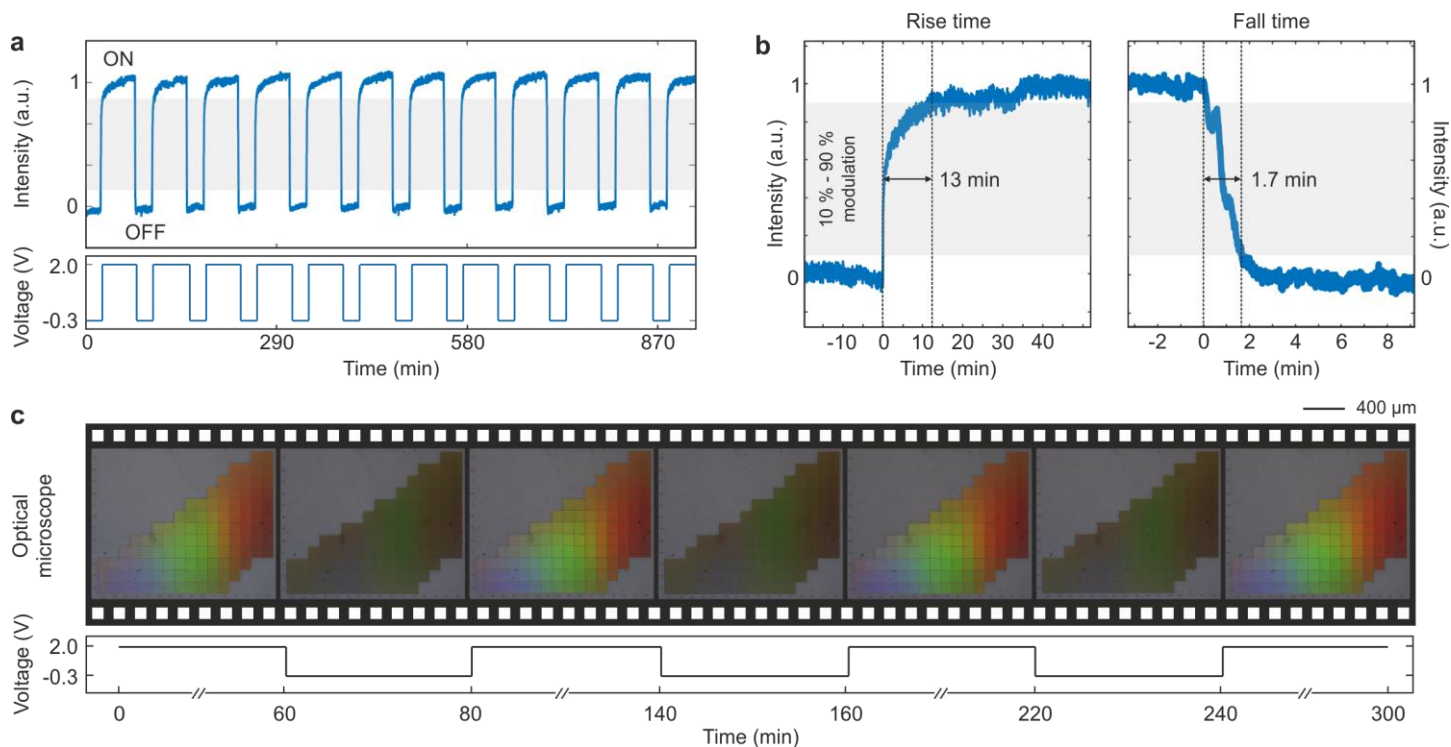


**Figure 2. Switching performance by electrical stimulation of  $\text{WO}_3$  metasurfaces.** (a) Transmitted intensity through the  $\text{WO}_3$  metasurface cycling between the ON and OFF states (Top). The gray area indicates the 10 % to 90 % modulation window. The voltage range is set between +2.0 V to -0.3 V (Bottom). (b) Detailed analysis of rise time  $\tau_{\text{rise}} = 13$  minutes (ON to OFF) and fall time  $\tau_{\text{fall}} = 1.7$  minutes (OFF to ON). The initial 50 % of the rise take place in 1.4 min. (c) Optical microscope images showing several cycles of colours switching ON and OFF when the applied voltage is cycled in situ between +2.0 V for 60 minutes to -0.3 V for 20 minutes.

The switching performance of our  $\text{WO}_3$  metasurfaces is investigated in Figure 2. The resonators are switched between ON and OFF states at applied voltages of +2.0 V and -0.3 V while tracking the transmitted intensity (see Methods for the detail). In Figure 2a, the modulated transmitted intensity is depicted in the top graph, corresponding to the voltage applied to the  $\text{WO}_3$  nanopatterns shown in the bottom graph. Twelve switching cycles are illustrated with a period of 80 minutes (20 minutes for OFF and 60 minutes for ON), confirming full switching between ON and OFF states without noticeable degradation (gray area: 10 % to 90 % modulation window).

Figure 2b displays the analysis of the rise time from ON to OFF (Left) and the fall time from OFF to ON (Right). The rise (or fall) time is defined as the time it takes for the transmitted intensity to rise (or fall) between 10 % and 90 %, respectively (dashed lines in figure 2b). We obtain a rise time ( $\tau_{\text{rise}}$ ) of 13 minutes and a fall time ( $\tau_{\text{fall}}$ ) of 1.7 minutes, resulting in a duty cycle time ( $\tau$ ) of

14.7 minutes. The initial 50 % of the switching during the rise take only around 1 minute. It is worth mentioning that the colour switching speed during the electrochemical reaction can be affected by several key factors including the thickness of  $\text{WO}_3$ , the cation concentration in an electrolyte, and the substrate temperature. In this work, 200 nm thick  $\text{WO}_3$ , acetonitrile containing 100 mM  $\text{LiClO}_4$  as an electrolyte, and room temperature are employed in all of the demonstrations. More detailed data on switching speed can be found in Figure S5 in the Supporting Information.

To visualize the switching performance of our metasurfaces, the images with a 5x objective are depicted in Figure 2c. Furthermore, movies that records the colour dynamics of the palette are presented in the Supplementary Movie 1 (for switching OFF) and Movie 2 (for switching ON). The colours generated by  $\text{WO}_3$  metasurfaces at a pristine state can be switched off upon lithium ion intercalation induced by an applied voltage of -0.3 V. Importantly, the colours of the palette can be nicely restored with a voltage of +2.0 V. This indicates that the  $\text{Li}_x\text{WO}_3$  are converted back to  $\text{WO}_3$ , therefore, displaying brilliant colours again. Such reversible switching is of high importance for dynamic applications.

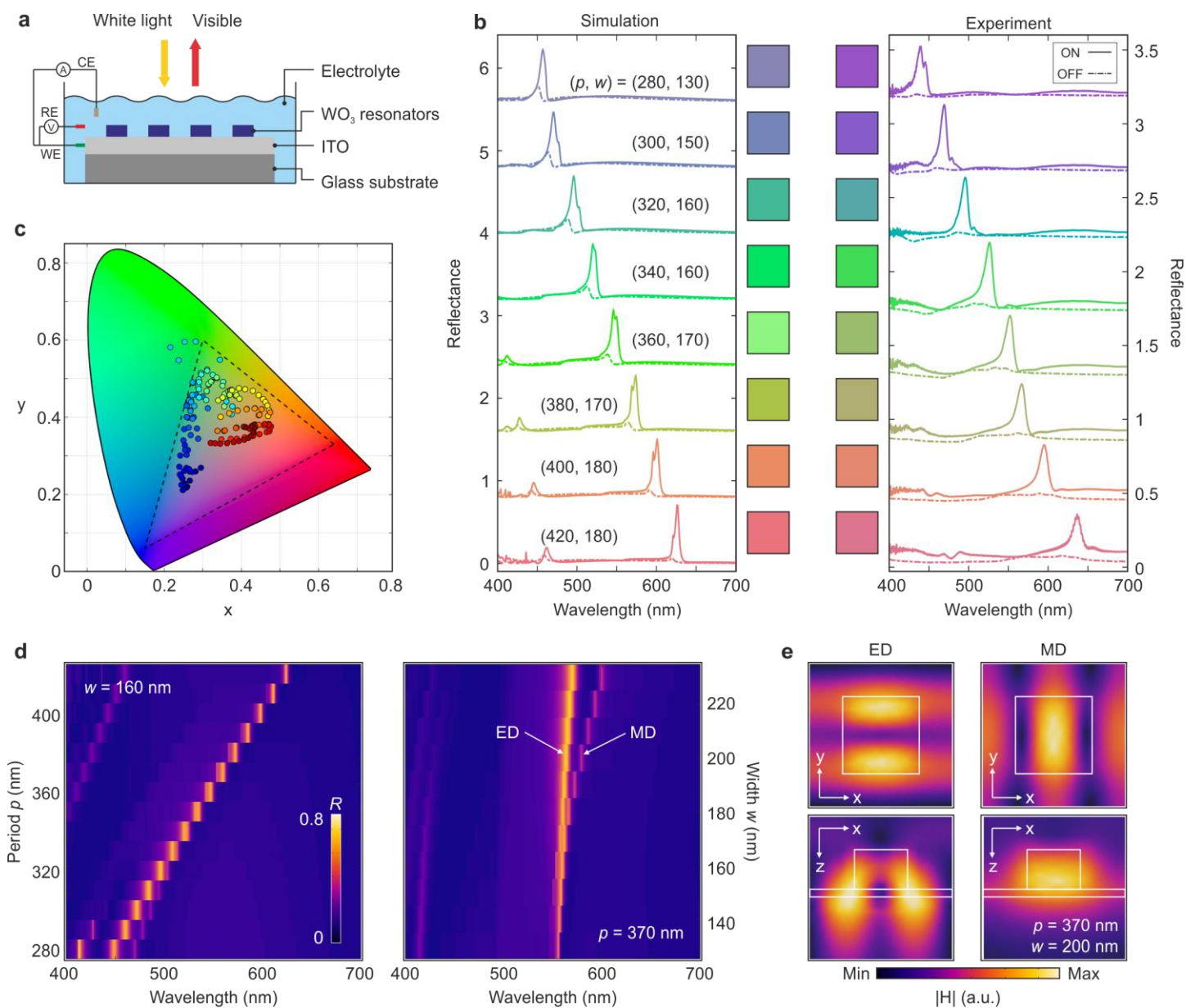


**Figure 3. Optical characterization of the colours from  $\text{WO}_3$  metasurfaces.** (a) Schematic of the electrochemical cell (three-electrode setup). The  $\text{WO}_3$  metasurface immersed in the electrolyte is illuminated by a white light source with normal incidence, and the reflected light is captured by an objective. (b) Simulated and experimental normal reflectance spectra for ON and OFF states. For the ON state, the colours corresponding to the reflectance spectra are depicted in the adjacent squares. (c) Measured reflectance spectra plotted in CIE 1931 colour map. A large colour gamut is obtained by varying the parameters of the metasurfaces (period  $p$  and width  $w$ ). The triangle formed by the dashed lines in the plot represents the standard RGB (sRGB) color space. (d) Simulated reflectance spectra as a function of wavelength for different periods or widths. (Left) With the width fixed to 160nm, high reflectance with narrow bandwidth is mainly depending on the period of nanostructures. (Right) Electric dipole (ED) and magnetic dipole (MD) resonances are observed depending on the widths with the period fixed to 370 nm. (e) The magnetic field

distributions of the cross-sections at the ED and MD resonances, respectively, in  $\text{WO}_3$  resonators with  $p = 370$  nm and  $w = 200$  nm.

Colour ON/OFF switching via external voltages is carried out in a liquid electrolyte using an electrochemical cell with a three-electrode system (Figure 3a; see Methods). For both ON and OFF cases, the spectral analysis of the representative colours among various structural information (period  $p$  and width  $w$ ) is carried out and presented in Figure 3b. The simulated spectra (left panel) indicate that the reflectance resonance has a high peak (around 70 %) with a narrow bandwidth, resulting in a high purity colour. Notably, the remaining reflectance which is slightly blue-shifted can be seen even in OFF state. It can be visually observed during the color change in Figure 2c (the colours are not completely ‘OFF’, and become slightly different). This is because our mechanism of ON/OFF switching is based on electrochromism of  $\text{WO}_3$ , which is the absorption tuning by electrical stimulus. The absorption coefficient of  $\text{WO}_3$  increased by electrochemical reduction is not sufficiently high to suppress the entire reflected intensity. The experimental reflectance spectra and their colours (Right panel) show an overall good agreement with respect to the simulation results. From the measured reflectance spectra, the structural colours that can be expressed through the combination of  $p$  and  $w$  of  $\text{WO}_3$  metasurfaces are displayed in the CIE 1931 colour space (Figure 3c).

To elucidate the underlying physics of the observed spectral characteristics, we numerically calculated the reflectance while varying  $p$  and  $w$ , respectively (Figure 3d). Above all, the reflectance peak clearly exhibits red-shifts with increasing period  $p$  (left panel), meaning the colours from our metasurfaces are mainly based on lattice resonance [34]. Also, we can observe the typical characteristics where the dipole resonance shifts according to the structural parameter  $w$  of the scatterers (right panel). Figure 3e depicts magnetic field distribution of the cross-section at the resonant peaks with  $p = 370$  nm and  $w = 200$  nm. From Figure 3e, we infer that the mode at shorter wavelength is the electric mode, whereas the long wavelength mode is the magnetic resonance. In principle, each  $\text{WO}_3$  nano-cuboid can support a Mie resonance due to its relatively high refractive index. However, its refractive index is not sufficiently high to be excited in a single resonator like silicon. In this sense, we arrange  $\text{WO}_3$  scatterers into periodic metasurfaces to enhance the reflectance efficiency due to the coupling effect between dipole resonances, and to suppress the other high-order resonant modes as a photonic band gap [13, 35].



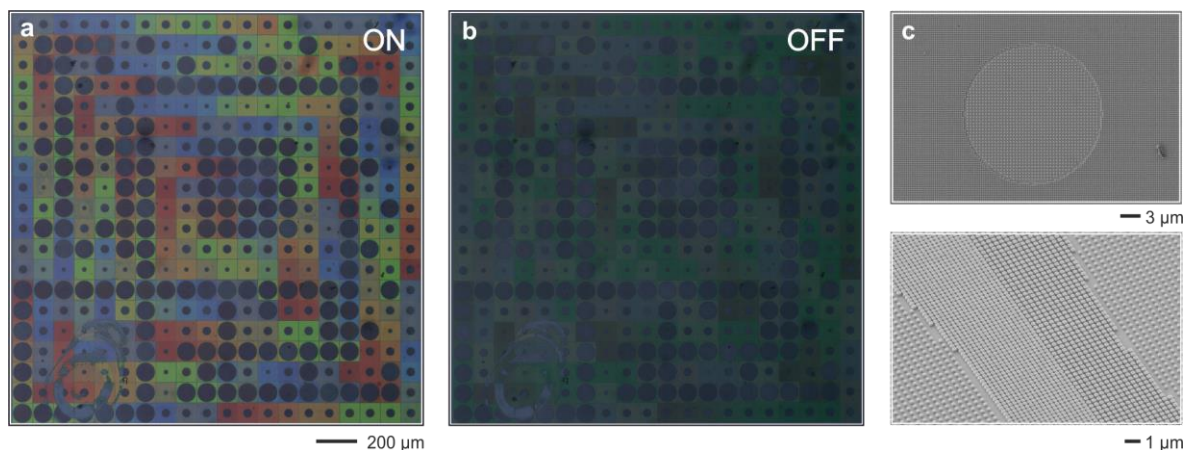


**Figure 4. Dynamic colour switching of arbitrary image.** (a) Optical microscopic image of the modified artwork, inspired by ‘Orion Gris’ of Victor Vasarely. Nanopatterned  $\text{WO}_3$  is ON state in electrochemically oxidized state. The size of whole pattern is 2 mm by 2 mm. (b) The artwork in OFF state during electrochemically reduced reaction for colour switching. (c) Enlarged SEM images of fabricated sample (Top: one square building block including a circle, Bottom: the edge between building blocks)

$\text{WO}_3$  metasurfaces have the potential to go beyond the light and thermal energy blocking capabilities of conventional smart windows [36], enabling the reproduction of arbitrary colour images and their ON/OFF switching. To demonstrate this ability, we proposed a millimeter-sized artwork as a blueprint inspired by Victor Vasarely’s *Orion Gris* (Figure 4a). The basic structure is a square shape containing a circle in the center. Each structure has circles of different sizes and backgrounds of different colours. Figure 4b represents the image erased into the OFF state for a dynamic switching. The SEM images of the basic structure and the edge area are shown in Figure 4c. It is worth mentioning that those SEM images were taken from the sample that already got switched on and off several times. This means that  $\text{WO}_3$  nanopatterns still exhibit no noticeable degradation during lithium ion intercalation and de-intercalation within a safe voltage range.

In summary, we have introduced novel active metasurfaces that operate in the visible spectrum. The high refractive index and electrochromic property of  $\text{WO}_3$  enable a high purity colour gamut with unprecedented subwavelength resolution and dynamic ON/OFF switching via applied voltages. Structural engineering and optimization of electrochemical environment can be carried out to further improve the switching speed and larger colour space for real world applications. Our concept will be of importance for solid-state devices with electrically tunable

optical responses and reflective displays, especially once the engineering task of addressing single pixels has been solved.

## **Methods**

### **Structure fabrication and characterization**

As substrate we use ITO (50 nm) coated glass to operate the ON/OFF switching of reflected colours and allow electrical addressability. A 200 nm layer of  $\text{WO}_3$  is deposited onto the substrate using reactive DC-magnetron sputtering (Star 100-TetraCo) with a metallic tungsten target. The deposition is performed with a power of 0.58 kW, a pressure of  $1.1 \times 10^{-2}$  mbar, and an Ar flow rate of 200 sccm, and an  $\text{O}_2$  flow rate of 70 sccm. The substrate was not heated and its temperature during deposition was below  $100^\circ\text{C}$ . The film is covered with a double-layered poly(methyl-methacrylate) (PMMA) positive tone resist (Allresist AR-P 642.06 200k, Allresist AR-P 672.02 950k), used to define nanostructures with electron beam lithography (EBL). After development in methylisobutylketone (MIBK), we use electron-gun evaporation to deposit a 30 nm Chromium (Cr) layer. After lift-off, Cr serves as hard-mask for the subsequent chemical etching process, which removes uncovered  $\text{WO}_3$ . The  $\text{WO}_3$  film is etched in a PlasmaPro80 etcher from Oxford with 100 W of radio-frequency power with an atmosphere of 10 sccm of  $\text{N}_2$ , 15 sccm of  $\text{CF}_4$ , and 10 sccm of  $\text{SF}_6$ . As a result, we obtain a  $\text{WO}_3$  metasurface after removing Cr via a commercial Cr remover. Scanning electron microscope images are taken with a Zeiss SEM Gemini 560.

### **Spectral measurements**

The presented reflectance spectra were measured in a setup based on an upright optical microscope (Nikon Eclipse LV). The exit path of the microscope is connected to the entrance slit of a Princeton Instruments grating spectrometer (Iso plane 160) with a Peltier-cooled CCD camera (PIXIS 256). The sample is placed on a motorized XY stage (Märzhäuser) and illuminated through the objective (Nikon TU Plan ELWD 20x, NA 0.4) by the in-built halogen white light lamp. We utilized internal apertures of the microscope to restrict the image plane (field stop) to the  $200 \mu\text{m}$  by  $200 \mu\text{m}$   $\text{WO}_3$  metasurface arrays. Additionally, the aperture in the microscope Fourier plane (aperture stop) is closed to restrict incident and collected light to angles close to normal incidence and blocking light scattered from the surrounding substrate. The measured spectra are normalized to the reflectance of a protected aluminum mirror (Thorlabs).

## **Numerical simulations**

Numerical simulations were carried out using commercial software COMSOL Multiphysics based on a finite element method. Periodic boundary conditions were used for calculation of the structure arrays. The refractive index of SiO<sub>2</sub> was taken as 1.47.

## **Electrochemical switching of metasurfaces**

We utilize a custom-built electrochemical cell to electrically switch the WO<sub>3</sub> metasurfaces using a three-electrode configuration. The cell is sealed with thin glass window at the top and bottom to allow optical access during reflectance/transmittance experiments. It includes side ports for electrolyte inflow and outflow, as well as connections for the reference and counter electrode. ITO (for electrical contact) underneath the WO<sub>3</sub> nanopatterns serves directly as the working electrode. The counter electrode is a platinum wire, and the reference electrode is silver/silver-chloride (Ag/AgCl), both in contact with 100 mM LiClO<sub>4</sub> electrolyte. A potentiostat (BioLogic SP-200) regulates the voltage over time. Temporal and switching characteristics are analyzed using a 633 nm He-Ne laser and a photodiode.

## **Author contributions**

Y.L conceived the original idea. Y.L., M.H. and H.G. supervised the work. Y.L. performed simulations and modelling for the WO<sub>3</sub> nanopatterns. A.G. provided WO<sub>3</sub> films. Y.L., M.U., and M.H. fabricated and characterized the samples. Y.L., J.H., and D.L. measured the colour samples. S.A. performed the spectroscopic measurements. All authors participated in the preparation and writing of the manuscript.

## **Acknowledgements**

This work was funded by Alexander von Humboldt Foundation (Y.L.), Bundesministerium für Bildung und Forschung (H.G.), Deutsche Forschungsgemeinschaft (GRK2642 Photonic Quantum Engineers; H.G.), European Research Council (ERC Advanced Grant Complexplas & ERC PoC Grant 3DPrintedOptics; H.G.), Carl-Zeiss-Stiftung (Center Qphoton, EndoPrint3D; H.G.). Also, this research was supported by Basic Science Research Program through the National Research Foundation of Korea (NRF) funded by the Ministry of Education (2021R1A6A3A14043838; Y.L.).

## References

1. Kelly, K. L., Coronado, E., Zhao, L. L. & Schatz, G. C. The optical properties of metal nanoparticles: the influence of size, shape, and dielectric Environment. *J. Phys. Chem. B* **107**, 668–677 (2003).
2. Biagioni, P., Huang, J.-S. & Hecht, B. Nanoantennas for visible and infrared radiation. *Rep. Prog. Phys.* **75**, 024402 (2012).
3. Barchiesi, D. Lycurgus Cup: Inverse problem using photographs for characterization of matter. *J. Opt. Soc. Am. A* **32**, 1544-1555 (2015).
4. Maier, S. A. & Atwater, H. A. Plasmonics: Localization and guiding of electromagnetic energy in metal/dielectric structures. *J. Appl. Phys.* **98**, 011101 (2005).
5. Kumar, K., Daun, H., Hegde, R. S., Koh, S. C. W., Wei, J. N. & Yang, J. K. W. Printing colour at the optical diffraction limit. *Nat. Nanotechnol.* **7**, 557–561 (2012).
6. Tan, S. J., Zhang, L., Zhu, D., Goh, X. M., Wang, Y. M., Kumar, K., Qiu, C.-W. & Yang, J. K. W. Plasmonic color palettes for photorealistic printing with aluminum nanostructures. *Nano Lett.* **14**, 4023–4029 (2014).
7. Clausen, J. S., Højlund-Nielsen, E., Christiansen, A. B., Yazdi, S., Grajower, M., Taha, H., Levy, U., Kristensen, A. & Mortensen, N. A. Plasmonic metasurfaces for coloration of plastic consumer products. *Nano Lett.* **14**, 4499–4504 (2014).
8. Knight, M. W., King, N. S., Liu, L., Everitt, H. O., Nordlander, P. & Halas, N. J. Aluminum for Plasmonics. *ACS Nano* **8**, 834-840 (2014).
9. Xue, J., Zhou, Z.-K., Wei, Z., Su, R., Lai, J., Li, J., Li, C., Zhang, T. & Wang, X.-H. Scalable, full-colour and controllable chromotropic plasmonic printing. *Nat. Commun.* **6**, 8906 (2015).
10. Kuznetsov, A. I., Miroshnichenko, A. E., Brongersma, M. L., Kivshar, Y. S. & Luk'yanchuk, B. Optically resonant dielectric nanostructures. *Science* **354**, 2472 (2016).
11. Proust, J., Bedu, F., Gallas, B., Ozerov, I. & Bonod, N. All-Dielectric Colored Metasurfaces with Silicon Mie Resonators. *ACS Nano* **10**, 7761–7767 (2016).
12. Flauraud, V., Reyes, M., Paniagua-Domínguez, R., Kuznetsov, A. I. & Brugger, J. Silicon nanostructures for bright field full color prints. *ACS Photon.* **4**, 1913-1919 (2017).
13. Sun, S., Zhou, Z., Zhang, C., Gao, Y., Duan, Z., Xiao, S. & Song, Q. All-dielectric full-color printing with TiO<sub>2</sub> metasurfaces *ACS Nano* **11**, 4445-4452 (2017).
14. Hentschel, M., Koshelev, K., Sterl, F., Both, S., Karst, J., Shamsafar, L., Weiss, T., Kivshar, Y. & Giessen, H. Dielectric mie voids: confining light in air. *Light Sci. Appl.* **12**, 3 (2023).
15. Decker, M., Staude, I., Falkner, M., Dominguez, J., Neshev, D. N., Brener, I., Pertsch, T. & Kivshar, Y. S. High-efficiency dielectric Huygens' surfaces. *Adv. Opt. Mater.* **3**, 813 (2015).
16. Duan, X., Kamin, S. & Liu, N. Dynamic plasmonic colour display *Nat. Commun.* **8**, 14606 (2017).
17. Byers, C. P., Zhang, H., Swearer, D. F., Yorulmaz, M., Hoener, B. S., Huang, D., Hoggard, A., Chang, W.-S., Mulvaney, P., Ringe, E., Halas, N. J., Nordlander, P., Link, S. & Landes, C. F. From tunable core-shell nanoparticles to plasmonic drawbridges: Active control of nanoparticle optical properties. *Sci. Adv.* **1**, e1500988 (2015).
18. Tsuboi, A., Nakamura, K. & Kobayashi, N. A localized surface plasmon resonance-based multicolor electrochromic device with electrochemically size-controlled silver nanoparticles. *Adv. Mater.* **25**, 3197 (2013).
19. Wang, G., Chen, X., Liu, S., Wong, C. & Chu, S. Mechanical chameleon through dynamic real-time plasmonic tuning. *ACS Nano* **10**, 1788 (2016).
20. Huang, M., Tan, A. J., Büttner, F., Liu, H., Ruan, Q., Hu, W., Mazzoli, C., Wilkins, S., Duan, C., Yang, J. K. W. & Beach, G. S. D. Voltage-gated optics and plasmonics enabled by solid-state proton pumping. *Nat. Commun.* **10**, 5030 (2019).
21. Li, N., Wie, P., Yu, L., Ji, J., Zhao, J., Gao, C., Li, Y. & Yin, Y. Dynamically switchable multicolor electrochromic films. *Small* **15**, 1804974 (2019).

22. Tseng, M. L., Yang, J., Semmlinger, M., Zhang, C., Nordlander, P. & Halas, N. J. Two-dimensional active tuning of an aluminum plasmonic array for full-spectrum response. *Nano Lett.* **17**, 6034 (2017).
23. Zhang, C., Jing, J., Wu, Y., Fan, Y., Yang, W., Wang, S., Song, Q. & Xiao, S. Stretchable all-dielectric metasurfaces with polarization-insensitive and full-spectrum response. *ACS Nano* **14**, 1418 (2020).
24. Liu, L., Aleisa, R., Zhang, Y., Feng, J., Zheng, Y., Yin, Y. & Wang, W. *Angew. Chem.* **131**, 16453 (2019).
25. Franklin, D., Frank, R., Wu, S.-T. & Chanda, D. Actively addressed single pixel full-colour plasmonic display. *Nat. Commun.* **8**, 15209 (2017).
26. Zhang, Y., Liu, Q., Mundoor, H., Yuan, Y. & Smalyukh, I. I. Metal nanoparticle dispersion, alignment, and assembly in nematic liquid crystals for applications in switchable plasmonic color filters and E-polarizers. *ACS Nano* **9**, 3097 (2015).
27. Greybush, N. J., Charipar, K., Geldmeier, J. A., Bauman, S. J., Johns, P., Naciri, J., Charipar, N., Park, K., Vaia, R. A. & Fontana, J. Dynamic plasmonic pixels. *ACS Nano* **13**, 3875 (2019).
28. Xu, T., Walter, E. C., Agrawal, A., Bohn, C., Velmurugan, J., Zhu, W., Lezec, H. J. & Tain, A. A. High-contrast and fast electrochromic switching enabled by plasmonics. *Nat. Commun.* **7**, 10479 (2016).
29. Xiong, K., Emilsson, G., Maziz, A., Yang, X., Shao, L., Jager, E. W. H. & Dahlin, A. B. Plasmonic metasurfaces with conjugated polymers for flexible electronic paper in color. *Adv. Mater.* **28**, 9956 (2016).
30. Lu, W., Jiang, N. & Wang, J. Active electrochemical plasmonic switching on polyaniline-coated gold nanocrystals. *Adv. Mater.* **29**, 1604862 (2017).
31. Peng, J., Jeong, H.-H., Lin, Q., Cormier, S., Liang, H.-L., De Volder, M. F. L., Vignolini, S. & Baumberg, J. J. Scalable electrochromic nanopixels using plasmonics. *Sci. Adv.* **5**, eaaw2005 (2019).
32. Lin, Y., Zheng, G., Xin, Q., Yuan, Q., Zhao, Y., Wang, S., Wang, Z.-L., Zhu, S.-N., Jiang, C. & Song, A. Electrically switchable and flexible color displays based on all-dielectric nanogratings. *ACS Appl. Nano Mater.* **4**, 7182 (2021).
33. Lee, Y., Yun, J., Seo, M., Kim, S.-J., Oh, J., Kang, C. M., Sun, H.-J., Chung, T. D. & Lee, B. Full-color-tunable nanophotonic device using electrochromic tungsten trioxide thin film. *Nano Lett.* **20**, 6084 (2020).
34. Castellanos, G. W., Bai, P. & Rivas, J. G. Lattice resonances in dielectric metasurfaces. *J. Appl. Phys.* **125**, 213105 (2019).
35. Babicheva, V. E. & Evlyukhin, A. B. Resonant lattice Kerker effect in metasurfaces with electric and magnetic optical resonances. *Laser Photonics Rev.* **11**, 1700132 (2017).
36. Granqvist, C. G. Electrochromism and smart window design. *Solid State Ion.* **53-56**, 479 (1992).

**Supporting Information**

**for**

**Inorganic electrochromic metasurface in the visible**

*Yohan Lee<sup>1\*</sup>, Jonas Herbig<sup>1</sup>, Serkan Arslan<sup>1</sup>, Dominik Ludescher<sup>1</sup>, Monika Ubl<sup>1</sup>, Andreas Georg<sup>2</sup>, Mario Hentschel<sup>1</sup>, and Harald Giessen<sup>1\*</sup>*

<sup>1</sup> 4th Physics Institute and Research Center SCoPE, University of Stuttgart, Pfaffenwaldring 57, 70569 Stuttgart, Germany

<sup>2</sup> Fraunhofer Institute for Solar Energy Systems, Heidenhofstraße 2, 79110 Freiburg, Germany

\*Corresponding author, e-mail: [y.lee@pi4.uni-stuttgart.de](mailto:y.lee@pi4.uni-stuttgart.de), [giessen@pi4.uni-stuttgart.de](mailto:giessen@pi4.uni-stuttgart.de)

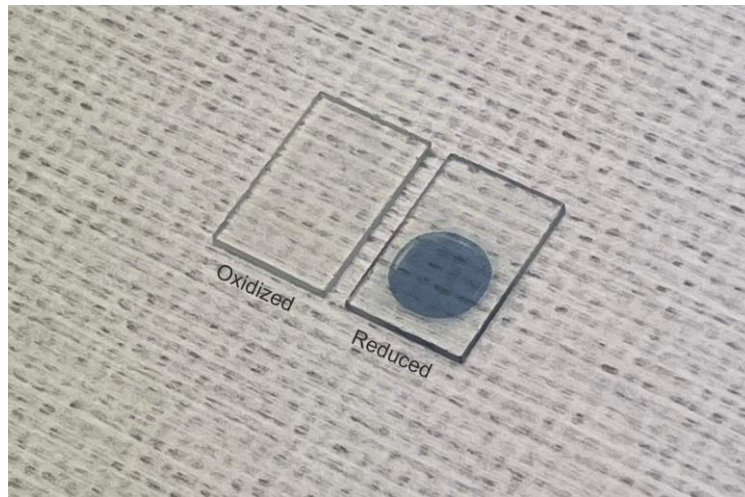


**Figure S1. Photograph of tungsten trioxide ( $\text{WO}_3$ ) thin films.** 200 nm thick  $\text{WO}_3$  films onto ITO-coated glass substrates in different electrochemical states: oxidized (left) and reduced (right).

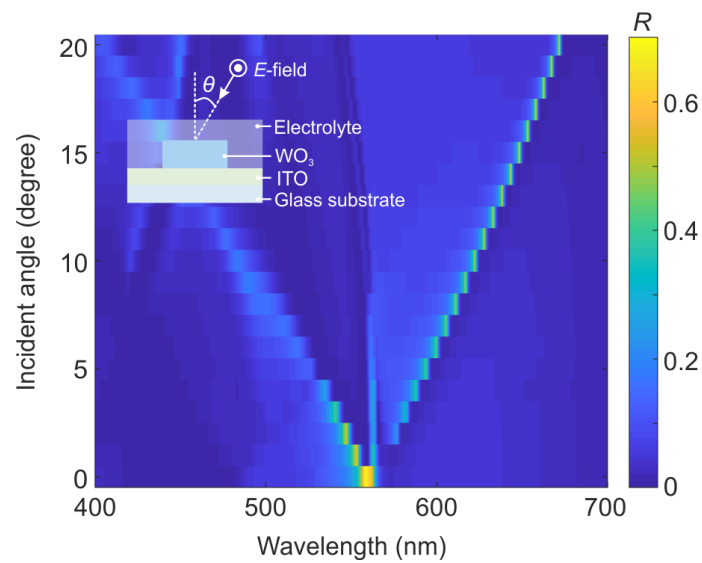


**Figure S2. Angle dependence of the  $\text{WO}_3$  metasurfaces.** The angle-dependent simulated reflectance spectra for TE-polarized incidence. The inset shows the angle and polarization of the incident light. The oblique incidence gives rise to the splitting of the normal incidence resonances of a  $\text{WO}_3$  metasurface. The oblique incidence disrupts the symmetry in the phase matching condition for forward and backward propagating Bloch waves of the metasurface.

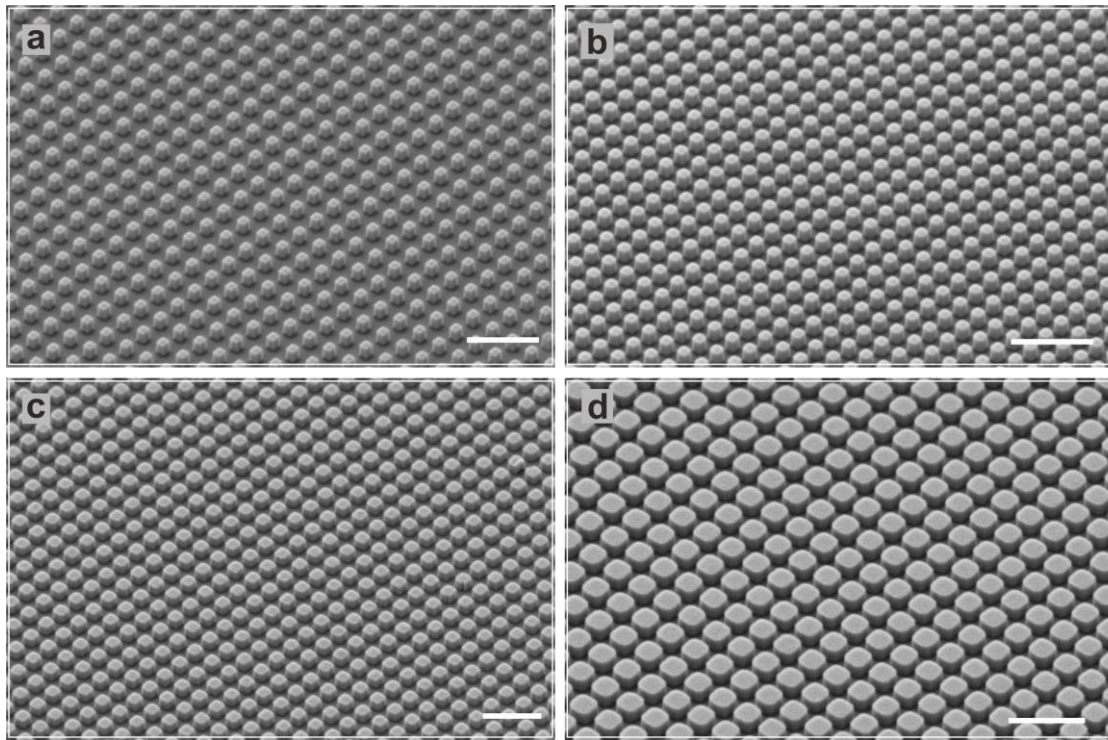


**Figure S3. Scanning electron microscopy (SEM) images of the  $\text{WO}_3$  metasurfaces.** The tilted-view SEM images of our  $\text{WO}_3$  metasurfaces with different unit sizes for various colours. The scale bars in (a) to (d) are all 1  $\mu\text{m}$ .

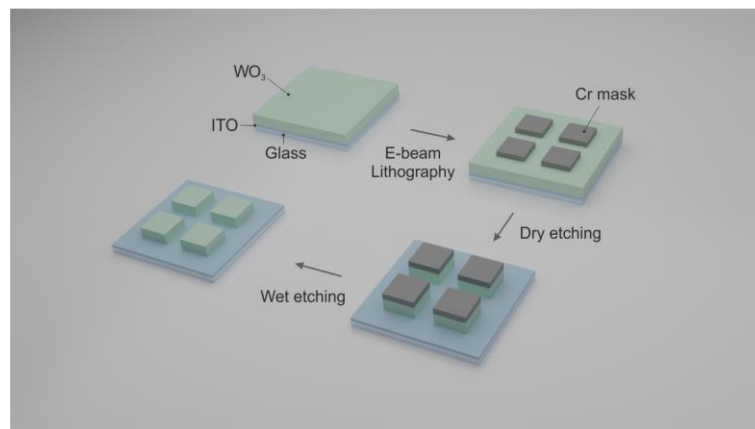


**Figure S4. Fabrication process of the  $\text{WO}_3$  metasurfaces.**  $\text{WO}_3$  thin film is deposited by RF sputtering onto a 50 nm indium-tin-oxide (ITO) coated glass substrate. The  $\text{WO}_3$  is then overcoated with PMMA, serving as a positive tone-resist for electron beam lithography. Following development, a 30 nm thick chromium (Cr) etch mask is deposited via electron-gun evaporation, and a standard lift-off in acetone is performed. Dry etching is carried out to remove the uncovered area, resulting in Cr-coated  $\text{WO}_3$  nanopatterns. After wet etching to remove the Cr mask, a  $\text{WO}_3$  metasurface is obtained.



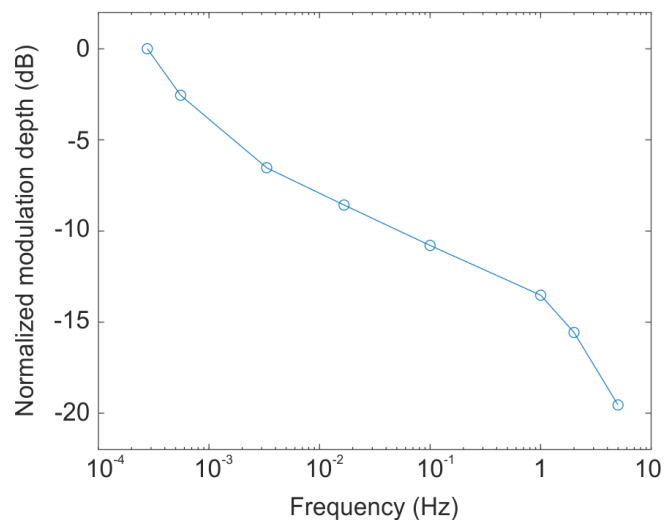


**Figure S5. Switching speed measurement.** Frequency characteristics of the WO<sub>3</sub> metasurfaces. The normalized modulation depth (defined the difference between maximum and minimum transmittance, normalized to the transmittance change value obtained over a period of 1 hour) as a function of input voltage frequencies.

**Table S1. Complex refractive indices of WO<sub>3</sub> for electrochemical states [1].**

Wavelength (nm)	Oxidized state		Reduced state	
	<i>n</i>	<i>k</i>	<i>n</i>	<i>k</i>
400	2.36088	0.00751	2.15122	0.09104
410	2.33499	0.00723	2.12438	0.09321
420	2.31245	0.00790	2.09828	0.09570
430	2.29110	0.00879	2.07557	0.09778
440	2.27486	0.00900	2.05310	0.10065
450	2.25785	0.00920	2.03204	0.10418
460	2.24315	0.00917	2.01329	0.10816
470	2.23006	0.00939	1.99436	0.11348
480	2.21756	0.00987	1.97593	0.12055
490	2.20728	0.01054	1.95940	0.12838
500	2.19720	0.01138	1.94335	0.13763
510	2.18900	0.01195	1.92949	0.14704
520	2.18180	0.01230	1.91593	0.15771
530	2.17481	0.01249	1.90443	0.16841

540	2.16945	0.01216	1.89332	0.18016
550	2.16354	0.01196	1.88354	0.19205
560	2.15945	0.01106	1.87500	0.20417
570	2.15437	0.01034	1.86741	0.21675
580	2.14989	0.00971	1.86061	0.22973
590	2.14583	0.00889	1.85482	0.24292
600	2.14206	0.00821	1.85019	0.25594
610	2.13823	0.00745	1.84656	0.26907
620	2.13563	0.00680	1.84344	0.28252
630	2.13250	0.00634	1.84138	0.29554
640	2.12977	0.00613	1.84011	0.30810
650	2.12738	0.00598	1.83931	0.32124
660	2.12436	0.00572	1.84001	0.33340
670	2.12205	0.00565	1.84050	0.34592
680	2.11948	0.00566	1.84160	0.35782
690	2.11813	0.00577	1.84300	0.36941
700	2.11579	0.00578	1.84579	0.38092

## References

1. Lee, Y., Yun, J., Seo, M., Kim, S.-J., Oh, J., Kang, C. M., Sun, H.-J., Chung, T. D. & Lee, B. Full-color-tunable nanophotonic device using electrochromic tungsten trioxide thin film. *Nano Lett.* **20**, 6084 (2020).